



Trans. Nonferrous Met. Soc. China 30(2020) 65-75

Transactions of Nonferrous Metals Society of China

www.tnmsc.cn



Microstructure, mechanical properties and two-body abrasive wear behaviour of hypereutectic Al–Si–SiC composite

Raj Kumar SINGH¹, Amit TELANG¹, Satyabrata DAS²

- 1. Department of Mechanical Engineering, Maulana Azad National Institute of Technology, Link Road Number 3, Bhopal 462003, India;
- 2. Advanced Materials and Processes Research Institute (AMPRI), Near Habibganj Naka, Bhopal 462026, India

Received 5 March 2018; accepted 24 October 2019

Abstract: The microstructure, mechanical properties, and the effects of sliding distance and material removal mechanism on two-body abrasive wear behaviour of hypereutectic Al–Si–SiC composite and its matrix alloy were investigated. The hypereutectic Al–Si–SiC composite was prepared by stir casting route. The hardness, ultimate tensile strength and yield strength of the composite are increased by 17%, 38%, and 30% respectively compared with those of the matrix alloy, while the elongation of the composite is decreased by 48% compared with that of the matrix alloy. The wear rate of the materials is increased with increasing the abrasive size and the applied load and does not vary with the sliding distance. The wear surfaces and wear debris of the materials were characterized by high-resolution field emission scanning electron microscopy (HR FESEM) and wear mechanism was analyzed for low and high load regimes.

Key words: metal matrix composite; fracture surface; debris analysis; two-body abrasive wear

1 Introduction

A high percentage of silicon-containing aluminium alloys has been utilized in a wide range of fields including automobile, defence and aerospace as a result of its properties like high thermal stability and low thermal expansion coefficient. The Al–Si alloys are immensely used for tribological applications, because of their process flexibility, low density and excellent formability [1–9]. The Al–Si alloys (containing hard Si particles dispersed with soft Al matrix) offer high strength, hardness and wear resistance compared with other alloys.

Some researchers [10–18] have been studied in different facets of Al–Si alloy and composite. SAWLA and DAS [10] found that the applied load of cast alloy decreased with an increase in wear

constant (K). The cast Al-Si alloy exhibits higher wear constant than the heat-treated alloy. DAS et al [11] observed that the Al-SiC composite has higher wear resistance in comparison with Al-Si matrix alloy in both as-cast and heat-treated conditions, irrespective of applied load and abrasive size. RAAFT et al [12] found that the A390-Al₂O₃ composite has higher wear resistance in comparison with the matrix alloy and A390-Gr composite. MONDAL and DAS [13] found that the ADC12-SiC composite has better wear resistance than its matrix alloy due to the addition of SiC particles. The wear rate increases with the increase of the applied load and does not vary with the abrasive size. SHAH et al [14] noted that the ageing temperature increased with an increase in the wear resistance. The hypereutectic Al-16%Si alloy has higher wear resistance compared with the eutectic Al-8%Si and hypoeutectic Al-12%Si alloys under

Corresponding author: Raj Kumar SINGH; E-mail: raju_tit@yahoo.co.in

DOI: 10.1016/S1003-6326(19)65180-0

similar conditions. SINGH et al [15] investigated the wear rate of an LM6 base alloy and sillimanite particle composite, which is enhanced by increasing the abrasive size, under an applied load with a reduced sliding distance. GODE et al [16] concluded that the Al-Si/5%SiC composite has lower dry sliding wear loss than its matrix alloy. LIN et al [17] found that the dry sliding wear rate of the Al-17Si alloy produced by rheocasting is lower than that of the conventionally produced alloy for the same applied load. In an applied load range of 50-200 N, wear rate of rheocast alloy increases. The combined action of oxidation and adhesion wear is responsible for the wear mechanism for the higher applied load. LI et al [18] found that hardness, ultimate tensile strength, elongation and wear resistance of the hypereutectic Al-Si alloy produced by the squeeze casting were higher than those of the alloy produced by gravity casting because of uniform dispersion of Si phase. From the literature survey, it is noted that most of the studies have mainly focused on processing and sliding wear response for hypereutectic Al-Si alloy, while no research work has been done on the correlation among microstructure, mechanical properties and abrasive wear behaviour of hypereutectic Al-Si alloy and its composite.

In the view of above, the aim of the present research was to study the microstructure, mechanical properties, the effects of sliding distance and material removal mechanism on two-body abrasive wear response of hypereutectic LM30–SiC composite and its matrix alloy. Additionally, the fracture surface, wear surfaces, and the wear debris were also examined through FESEM.

2 Experimental

2.1 Materials preparation

The hypereutectic Al–Si (BS: LM30) alloy and LM30–SiC_p composite were chosen in the present work. An optical emission spectrometer (SPECTRO MAXx LMF05, SPECTRO, Germany) was used for the verification of the chemical composition of the alloy and composite. The chemical compositions of the alloy and composite are shown in Table 1. The synthesis process of Al alloys was melting of aluminium at 850 °C, mixing silicon and another alloying element to form LM30 alloy, stirring and

degassing, and finally casting into a permanent die. The composite was reinforced with 10 wt.% SiC particles with a size of 20–40 μm (Grindwell Norton Ltd., Bangalore, India). The LM30–SiC $_p$ composite was prepared by stir casting route, and the process was melting the aluminium alloy at 850 °C, stirring the melt through a mechanical stirrer, adding dispersoids in the melt and finally casting into a permanent cast iron die.

Table 1 Chemical compositions of specimens

C	Content/wt.%							
Specimen	Si	Mn	Mg	Cu	Fe	Ni	SiC	Al
LM30 matrix alloy							-	
LM30-10wt.%SiC composite	17.5	0.3	0.6	4.5	1	0.1	10	Bal.

2.2 Particle size analysis

SiC particle size analysis in as-received conditions was carried out by Maser Swizer S (version 21.5) analyzer (Malvern Instruments Limited, Enigma Business Park, Grovewood Road, UK). Laser technology was used in this analyzer, which was also known as a laser diffraction technique. The result was expressed in terms of the size range of particles and percentage frequency of particles.

2.3 Density and hardness measurement

The density of the alloy and composite was measured by using the Archimedes principle of water displacement method. The hardness of alloy and composite was measured by a Vickers hardness testing machine (VM 50, FIE Pvt. Ltd., Maharashtra, India). The specimen was polished metallographically and made perfectly parallel on the opposite side before hardness measurement. The Vickers hardness of the sample was obtained by using a diamond pyramid indenter with an applied load of 300 N at a dwell time of 5 s. Ten hardness readings were taken, and an average value was reported.

2.4 Tensile tests

Tension tests were conducted on specimens with 10 mm in diameter and 50 mm in gauge length as per IS 1608. The experiments were performed at room temperature using a computerized tension-testing machine with a capacity of 300 kN (5586,

Instron, Norwood, MA, USA). A strain rate of 0.01 s⁻¹ was used. The ultimate tensile strength, 0.2% proof stress (yield strength) values and elongation were recorded.

2.5 Two-body abrasive wear test

The two-body abrasive wear tests were performed on a Suga abrasion tester (NUSI, Suga Test Instruments Co., Ltd., Shinjuku-ku, Tokyo, Japan). A self-adhesive silicon carbide abrasive paper of different sizes was cut into the appropriate size and bonded with a rotating wheel (width: 10 mm; diameter: 50 mm) to act as the abrasive medium. The dimensions of rectangular specimens were 40 mm \times 35 mm \times 5 mm. The mass loss of the sample was measured after every 400 cycles (corresponding sliding distance: 27 m). After every 400 cycles, the fresh abrasive paper was used so that the wear track was always subjected to fresh abrasive [19]. Before and after the wear tests, the specimens were cleaned with acetone and weighed with a microbalance. The mass loss values were converted into volume loss values, which were used for the wear rate calculations. The wear rate was expressed in terms of the volume loss per unit sliding distance. For each condition, the tests were performed three times, and the average value was taken. The wear tests were conducted at a sliding distance from 27 to 108 m, a self-adhesive silicon carbide abrasive paper size of 40–80 μ m and an applied load of 1–7 N.

2.6 Microstructural observation

To study the microstructures, specimens were polished with the standard metallographic practice and then etched by Keller's reagent. The etched specimens were examined using a high-resolution field emission scanning electron microscope (Ultra Plus, Carl Zeiss Microscopy GmbH, Oberkochen, Germany) operating at 20 kV. The specimens were sputtered with the gold coating before high-resolution field emission scanning electron microscopy (HR FESEM). The fracture surface, wear surface and debris particles were also studied by HR FESEM.

3 Results

3.1 Microstructure

The morphology of the particles was examined through scanning electron microscope (5600, JEOL Ltd., Akishima, Tokyo, Japan), as shown in Fig. 1(a). It shows the nature of equiaxed particles with sharp edges. The microstructure of matrix alloy mainly consists of primary aluminium, eutectic silicon, and primary silicon particles. It has

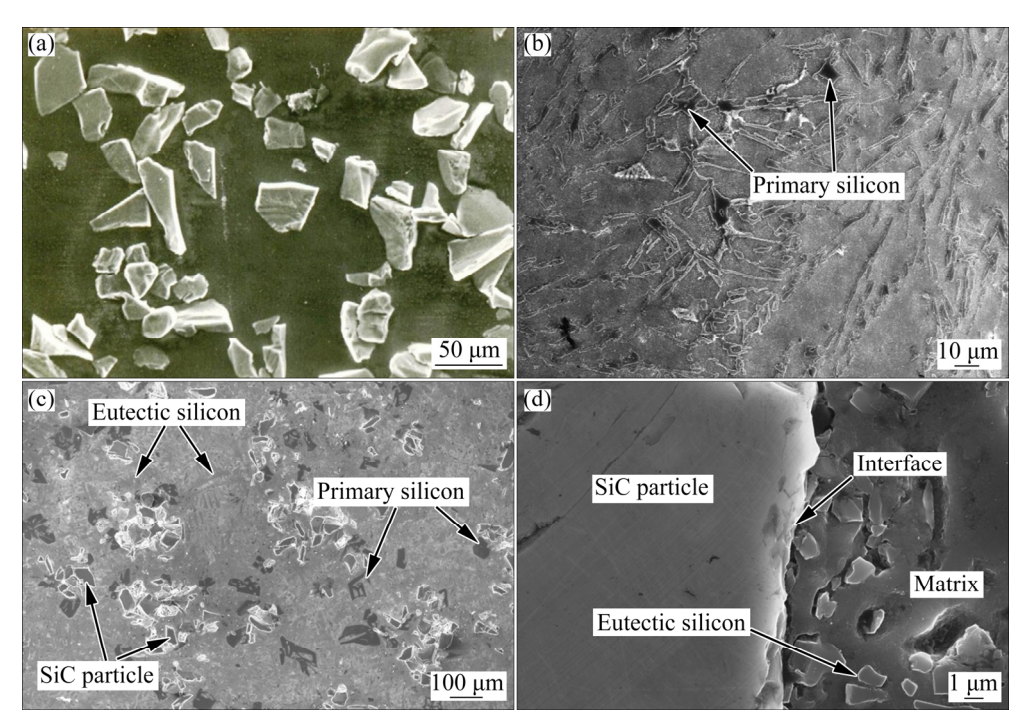


Fig. 1 Morphology of SiC reinforcement (a), higher magnification microstructures of LM 30 alloy (b) and LM30–10%SiC composite (c), and micrograph showing interfacial bonding between SiC particle and metallic matrix (d)

been found that the eutectic silicon appeared as coarse needle-shape and dispersed with primary silicon cuboids, as shown in Fig. 1(b). Figure 1(c) shows the microstructure of LM30–10%SiC composite, which exhibits uniform dispersion of SiC particles in an aluminium matrix. Figure 1(d) shows a typical micrograph of the interface depicting the excellent bonding strength between the SiC particles and aluminium matrix.

3.2 Particles size distribution

The size range of silicon carbide particles was represented by the histogram and is shown in Fig. 2. It depicts that 23% particles are in size range of 20–25 μ m, 55% particles are in size range of 25–30 μ m, 14% particles are in size range of 30–35 μ m and 8% particles are in size range of 35–40 μ m. It is evident from Fig. 2 that the maximum distribution of SiC particles (55%) was obtained in the size range of 25–30 μ m.

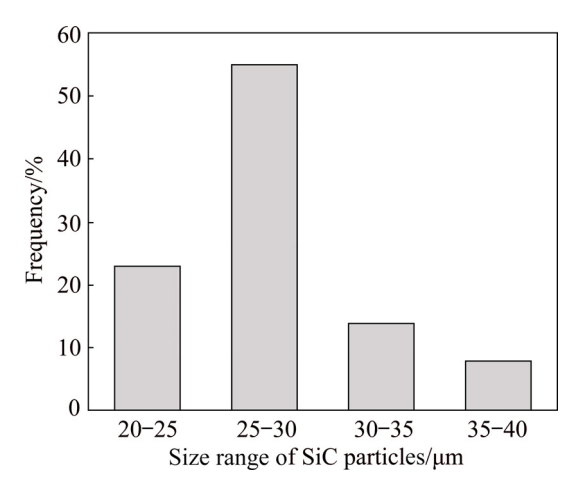


Fig. 2 Particle size distribution of SiC particles

3.3 Density and hardness

Table 2 shows the densities and hardnesses of the matrix alloy and composite. The densities of LM30 alloy and LM30–10%SiC composite were recorded to be 2.71 and 2.8 g/cm³, respectively. The silicon carbide has a higher density than the aluminium alloys. For this reason, the density of the

composite is higher than that of matrix alloys. The hardness of the composite is 17% greater than that of the matrix alloy, as a result of adding SiC_p to the matrix.

3.4 Tensile properties

The ultimate tensile strength (UTS), yield strength (YS) and elongation of the matrix alloy and composite are also shown in Table 2. The UTS and YS of the composite are 38% and 30% greater than those of the matrix alloy, respectively. The elongation of the composite is 48% less than that of the matrix alloy.

3.5 Two-body abrasive wear

Figure 3 shows the abrasive wear rate of the materials as a function of sliding distance at different abrasive sizes. The wear rate of LM30-10%SiC composite is compared with that of LM 30 alloy in terms of the sliding distance. Figure 3(a) shows that, at a abrasive size of 40 µm, an applied load of 1 N and a sliding distance of 27 m, the wear rates of LM30 alloy and LM30-10%SiC composite are 4.5×10^{-11} and 1.6×10^{-11} m³/m, respectively. For a sliding distance of 108 m, the wear rates of LM30 alloy and LM30–10%SiC composite are 5.19×10⁻¹¹ and 1.36×10⁻¹¹ m³/m, respectively. The wear rates decrease to around 64.44% and 73.8% at sliding distances of 27 and 108 m, respectively. In the case of abrasive size of 40 µm, applied load of 7 N and sliding distance of 27 m, the wear rates of LM30 alloy and LM30–10%SiC composite are 18.7×10⁻¹¹ and 6.7×10^{-11} m³/m, respectively. At a sliding distance of 108 m, the wear rates of LM30 alloy and LM30-10%SiC composite are 19.31×10⁻¹¹ and $7.10 \times 10^{-11} \,\mathrm{m}^3/\mathrm{m}$, respectively. The wear rates decrease to around 64.17% and 63.23% for sliding distances of 27 and 108 m, respectively.

Figure 3(b) shows that at an abrasive size of 65 μ m, an applied load of 1 N and a sliding distance of 27 m, the wear rates of LM30 alloy and LM30–10%SiC composite are 5.4×10^{-11} and

Table 2 Physical and mechanical properties of specimens

Specimen	Density/(g·cm ⁻³)	Hardness (HV)	UTS/MPa	YS/MPa	Elongation/%
LM30 matrix alloy	2.71	126	210	185	1.8
LM30-10%SiC composite	2.8	147	290	240	0.95

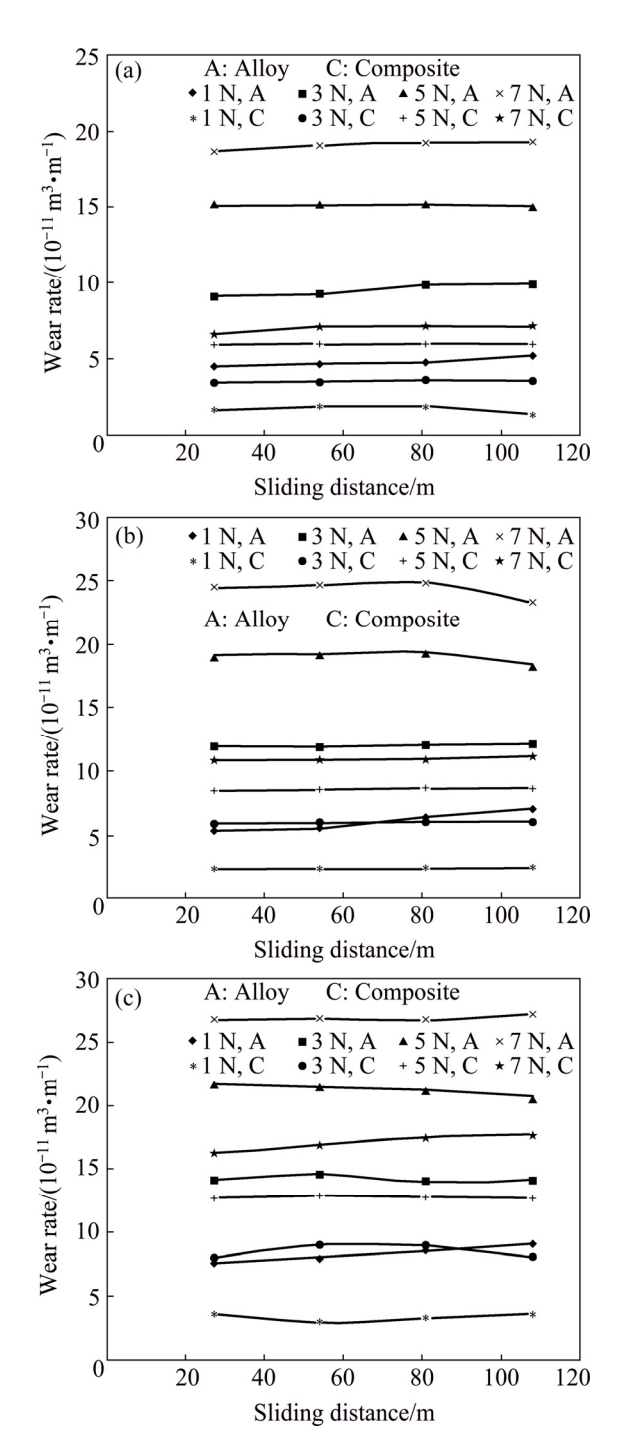


Fig. 3 Wear rate as function of sliding distance at different abrasive sizes of 40 μ m (a), 65 μ m (b) and 80 μ m (c)

 $2.36\times10^{-11}\,\mathrm{m}^3/\mathrm{m}$, respectively. At a sliding distance of $108\,\mathrm{m}$, the wear rates of LM30 alloy and LM30– $10\%\mathrm{SiC}$ composite are 6.94×10^{-11} and $2.37\times10^{-11}\,\mathrm{m}^3/\mathrm{m}$, respectively. The wear rates decrease to around 56.3% and 65.85% at sliding distances of 27 and $108\,\mathrm{m}$, respectively. While in the case of an abrasive size of $65\,\mu\mathrm{m}$, an applied load of $7\,\mathrm{N}$, and a sliding distance of $27\,\mathrm{m}$, the

wear rates of LM30 alloy and LM30–10%SiC composite are 24.4×10^{-11} and 10.8×10^{-11} m³/m, respectively. At a sliding distance of 108 m, the wear rates of LM30 alloy and LM30–10%SiC composite are 23.4×10^{-11} and 11.1×10^{-11} m³/m, respectively. The wear rates decrease to around 55.74% and 52.56% at sliding distances of 27 and 108 m, respectively.

Figure 3(c) shows that at an abrasive size of 80 μm, an applied load of 1 N and a sliding distance of 27 m, the wear rates of matrix alloy and composite are 7.56×10^{-11} and 3.5×10^{-11} m³/m, respectively. At a sliding distance of 108 m, the wear rates of LM30 alloy and LM30-10%SiC composite are 8.91×10^{-11} and 3.53×10^{-11} m³/m, respectively. The wear rates decrease to around 53.7% and 60.38% at sliding distances of 27 and 108 m, respectively. In the case of an abrasive size of 80 µm, an applied load of 7 N, and a sliding distance of 27 m, the wear rates of matrix alloy and composite are 26.7×10^{-11} and 16.2×10^{-11} m³/m, respectively. At a sliding distancees 108 m, the wear rates of LM30 alloy and LM30-10%SiC composite was 27.18×10^{-11} and 17.7×10^{-11} m³/m, respectively. The wear rates decrease around 39.33% and 34.88% for sliding distances of 27 and 108 m, respectively.

4 Discussion

4.1 Microstructure

The microstructure of the LM30 alloy features aluminium dendrites and eutectic silicon in the interdendritic region and around the dendrites. The eutectic silicon, which is needle-shaped, grows isotropically as a result of a twin-plane re-entrant edge (TPRE) mechanism. The silicon needles grow straight for some distances and then turn through a large angle by multiple entwining and then branching off to form a coarse-faceted shape. The sharp edges of the eutectic silicon act to increase the stress such that cracks nucleate easily at the edges of the silicon. The distribution of the reinforcement in a metallic matrix depends on the wettability between the matrix and ceramic phase and the difference between the densities of the metallic matrix and ceramic phase. If the density differences are higher, there will be a tendency for the reinforcing particles to either settle down or float.

In the case of Al-Si composite, the density of aluminium is 2.70 g/cm³; whereas the density of SiC particulate is 3.4 g/cm³. As the SiC particle is denser than the aluminium melt, there is a tendency for SiC particle to settle down during the solidification. Thus, to achieve uniform dispersion of SiC particle in aluminium alloy matrix, the composite melt is to be solidified as fast as possible so that the particles do not get enough time to settle down. In the present investigation, the crosssection of the casting (along with the length) and the distribution of the particle from top to bottom are observed to be quite uniform. During solidification of the Al-Si-SiC composite, the SiC particles are pushed by the primary aluminium dendrites to the last freezing eutectic liquid. The primary Al phases, the SiC particle in the last freezing eutectic liquid and therefore the particles are observed in the inter-dendritic regions and around the dendrites. So, eutectic silicon is always found around the SiC particles. During eutectic solidification, eutectic silicon may nucleate first at the SiC/melt interface.

4.2 Fracture surface

Figures 4(a, b) show the tensile fracture morphologies of the matrix alloy and composite, respectively. The fracture of the silicon occurs in a brittle mode having no or negligible plastic deformation (i.e., only low specific surface energy is required to produce a new fracture surface); whereas aluminium fractures in the ductile mode because there is a significant amount of plastic deformation (i.e., requiring high specific surface energy to produce a new fracture surface). Fracture surface studies of the Al-Si alloys reveal brittle fracture consisting of trans-granular cleavage facets (which fracture through the grains/silicon particles), as shown in Fig. 4(a). The primary silicon particles are responsible for crack initiation and propagation. On the other hand, Fig. 4(b) indicates that the fracture surface of the composite is composed of a significant amount of cleavage fracture and only a few microcracks (denoted by the circle in Fig. 4(b)). It also reveals the formation of cavities resulting from the SiC particles being pulled out from the matrix during tensile loading, with the SiC particles fracturing due to the excellent interfacial bonding between the SiC particles and the Al matrix. The fracture surface of the composite exhibits a river

line pattern (denoted by "A" in Fig. 4(b)), the direction of which is towards the origin of the crack. As a result, the Al-Si alloy exhibits superior ductility (that is, toughness), relative to that of the composite.

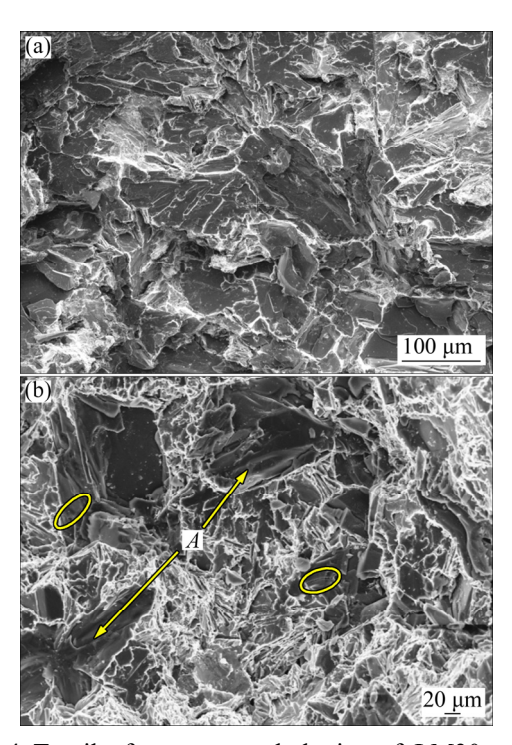


Fig. 4 Tensile fracture morphologies of LM30 matrix alloy (a) and LM30–10%SiC composite (b)

4.3 Effect of sliding distance on two-body abrasive wear

For a composite, the wear rate does not follow any specific relation with sliding distance. Figure 3 shows that the wear rate does not obviously vary with the sliding distance. The composite material is significantly harder, and the SiC particles of the composite strongly protect the softer matrix, especially at a lower applied load. The penetration depth is considerably low for lower applied load, and the surface topography does not vary with an increase in the sliding distance. Thus, the wear rate of composite remains almost constant with sliding distance, especially in low load condition. When the load increases, the penetration depth of the abrasives on the specimen surface is increased. As the sliding distance increases, the abrasives penetrate more deeply into the region. Therefore, due to the higher penetration depth, wider grooves are produced and the possibility of debonding of particles increases. At the same time, the chances of fracture and fragmentation of the hard dispersoids

and the flaky materials along the wear tracks increase with an increase in sliding distance. Wear is associated with the surface-to-surface contact and ability of the asperities of the counter surface (in this case abrasive particles) to penetrate into the specimen surface and scratching under load. Initially, the asperity-to-asperity contact is less, so the work hardening is also less. Thus, the applied load is shared by less number of asperities of the specimen as well as the counter surface. Consequently, for a given applied load, each of the asperities is subjected to the higher stress level, causing more considerable damage to the specimen surface. However, at the same time, some abrasives coming in contact with the specimen are also less. As a result, wear groove formation is also less. With the increase in sliding distance, asperity-to-asperity contact becomes more efficient, which may lead to higher wear rate by removing more materials. After a specific sliding distance, asperity (of the specimen) to abrasive (of the abrasive medium) contact reaches the most efficient regime, and it does not change further with increasing sliding distance. However, the work hardening may improve further with sliding distance because of a higher degree of deformation. Surface cracks are also generated in longitudinal and transverse directions, which in due course cause significant damage to the wear surface. This leads to higher wear rate which may nullify the

effect of work hardening of wear surface. As a result, the wear rate throughout the entire range of sliding distance remains more or less same when one uses fresh abrasive every time.

4.4 Material removal mechanism during twobody abrasive wear

In the abrasive wear, soft material of alloy and composite is scratched by abrasive paper embedded with SiC particle. Hard SiC particle which is embedded in the paper penetrates into the soft matrix. During reciprocating motion, the soft undergoes ploughing material as microcracking action. In the case of an alloy, silicon is a hard phase embedded in the aluminium matrix observed as coarse faceted shaped particles which tend to fracture into smaller equiaxed shaped ones. During the wear process, continuous scratching (abrasion action) forms a mixed layer of aluminium and fractures Si particles which are seen in Figs. 5(a, b) during the abrasive wear process due to the applied load. Crack is initiated at the Al/Si interface because of higher stress concentration and propagates at the interface between the lessdeformed material and the mixed layer. Abrasive wear takes place in several simultaneous stages. Firstly, the coarse faceted shaped hypereutectic silicon in which the crack nucleated at the Al/Si interface grew transversely and longitudinally along

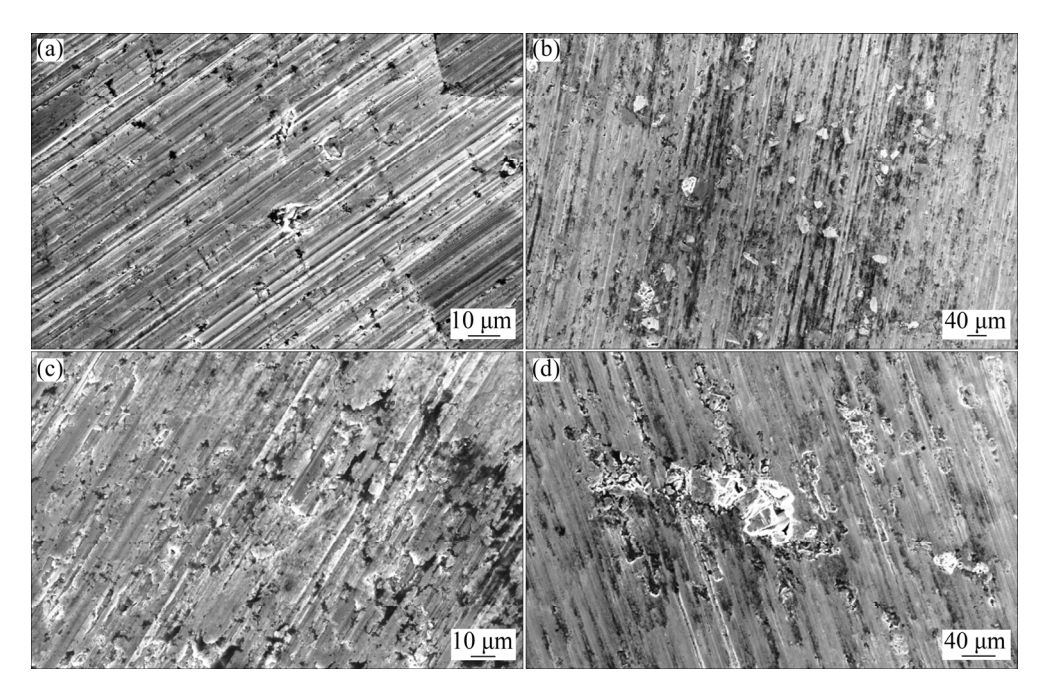


Fig. 5 Wear surfaces of LM30 matrix alloy and LM30–10%SiC composite at sliding distance of 108 m: (a, b) Applied load of 1 N and abrasive size 40 μm; (c, d) Applied load of 7 N and abrasive size of 80 μm

with the interface of the less-deformed and mixed layer which finally interconnected together in the aluminium matrix; secondly, the hypereutectic silicon was distributed in Al matrix. The near shape of silicon particle considerably reduces the stress concentration effect and vis-à-vis crack nucleation. In the case of composite, the dispersed SiC particles which are embedded in the Al matrix, improve the wear resistance by protruding the particles on the wear surface. Such particles resist further wear of the material. However. during continuous reciprocating motion, the stress developed at the interface of SiC particle and Al matrix is more, and ultimately there is every possibility that cracks nucleate and propagate, and join with the crack generated around the other particle. Such a situation results in a surface consisting of highly deformed Al-Si mixed layer, on which SiC particles are embedded. It also appears that during the continuous scratching, the stress developed in SiC particles leads to breaking at the edges of the particle. It is conceivable that during abrasive wear at the low load, the stress applied to the particle is less, and the possibility of fracturing of particles is negligible, and only the edges of the particles usually break. There is specific material removal mechanism during abrasive wear of composite in low load regime. At the initial stage of abrasive wear, the soft aluminium is just worn out, leaving behind the SiC particles. This result is in protrusion of SiC particles on the mating surface. During the continuous abrasion, highly deformed Al-SiC mixed layer is formed, and at the same time, the high cyclic stress is developed at the interface of SiC particle and Al matrix, which leads to crack initiation especially the boundary between the mixed layer (severely deformed layer and less-deformed layer) and propagation preferentially in the longitudinal direction. The crack nucleation mainly depends upon the strength of the interface between SiC particle and Al matrix (if any intermetallic phases are formed). However, in the present observation, there is no evidence of formation of intermetallic phase at the interface. Hence, the crack nucleation solely depends upon the interface bonding between Al and SiC, which is essential of the mechanical type. Then, crack propagates along the boundary of the mixed layer and less-deformed layer, finally joining with each other and causing fragmentation of SiC particles

and matrix. It may be noted that in low load regime, the SiC particles do not fracture and remain intact in the mixed layer, leading to considerable improvement in wear resistance over unreinforced alloy. However, in high load regime, there are probabilities of cracking and fracturing of particles, and there is again a perfect material removal mechanism developing in SiC particles, which leads to breaking at the edges of the particles. Material removal mechanism during abrasive wear of composite in high load regime is that the distribution of SiC particles and crack initiation and growth on the particle are due to high-stress accumulation. Then, there is the removal of the broken particle, and there is fragmentation of SiC particles into smaller sizes and subsequent removal. Such SiC particle fragmentation depends on the stress level, rather than cycles and abrasive size. It would be observed that the interface of SiC particle and Al matrix gets plastically deformed because of plastic inconsistency between the matrix and SiC particle. Thus, a plastic environment is developed near the particles, which increases the development of cracks along the interface of SiC particle and Al matrix. At higher applied load and coarser abrasive size, the penetration depth is more as shown in Fig. 5(c). The matrix material gets deformed due to rubbing action and is spread over the SiC particles. As a result, protruded SiC particles are not observed on the wear surface. Because of reciprocating motion and plastic inconsistency between SiC particle and Al matrix, the thin layer of matrix material over the SiC particles gets removed after a prolonged sliding distance, and a situation takes place when the SiC particles are exposed as protruded particles over the specimen surface. As a result of fatigue type of deformation, debonding and fracture of SiC may take place. For higher applied load and coarser size of abrasive, the material is removed due to cutting, ploughing and micro-fatigue cracking, as shown in Fig. 5(d). Consequently, the SiC particles are exposed in the initial stage. After a prolonged sliding distance, these particles are fragmented and scooped off from the wear surface. The cycles of the covering of SiC particles with matrix material, the matrix material removal from the surface of SiC particles and fracturing and removal of the SiC particles continue during abrasive wear of composite [20]. It may be concluded from the present investigation that the

two-body abrasive wear of composite mainly relies on the applied load and abrasive size. In low load regime, a mixed layer of Al, Si and SiC is formed, which in turn gets detached from the wear surface during the wear process. SiC particles are found to be intact in the mixed layer without fracturing. However, in high load regime, the SiC particles in the matrix are cracked due to the concentric load applied to the particles. In addition to the formation of the mixed layer, cracking of particles is observed. The present work demonstrates two distinct mechanisms of material removal based on the applied load, during abrasive wear of Al-Si-SiC composite. In low load condition, the formation of the mixed layer is the predominant mechanism, and in high load regime, particle fracturing is the dominating factor to control the wear of materials. Larger abrasive size particles (larger than the size of reinforcement) either scoop off the reinforcement or fracture.

4.5 Wear debris analysis

The wear debris of the matrix alloy and composite was examined by FESEM in an attempt to determine the mechanism of material removal in the abrasive wear process. FESEM images of the debris of matrix alloy and composite at an abrasive size of 80 µm and an applied load of 7 N are shown in Figs. 6(a, b), respectively. The penetration depth of the abrasive particles on the specimen surface depends on the attack angle (rake angle) of the cutting edge [21], the degree of contact stress [22], the hardness of material surface [22], and the abrasive size [21,22]. The penetration depth increases with the increase in the rake angle, abrasive size and applied load (Fig. 3), and also increases the increase of the wear rate while decreases with an increase in hardness of specimen surface. Due to these facts, for the coarser abrasive size and higher applied load, matrix alloy and composite sustain higher wear rates as shown in Fig. 3(c), as well as longer and wider flakes, as shown in Fig. 6. For the alloy, the majority of the wear debris particles are found to be deformed machining chips and flakes. In the case of the composite, the wear debris consisted of flakes and machining chips, along with the fragmented particles [23]. The debris became coarser with an increase in the size of abrasives and the applied load [24]. The formation of flakes depends upon the microplouhing and micro-cutting process. The formation of larger debris size, longer machining chips and deformed flakes in the wear debris of the alloys could be a result of the higher ductility of the alloy than the composite [21,25,26], as shown in Fig. 6. Less wear surface damage, finer debris formation and more capping, clogging, and attrition of the abrasive led to a lower wear rate and vice versa [23].

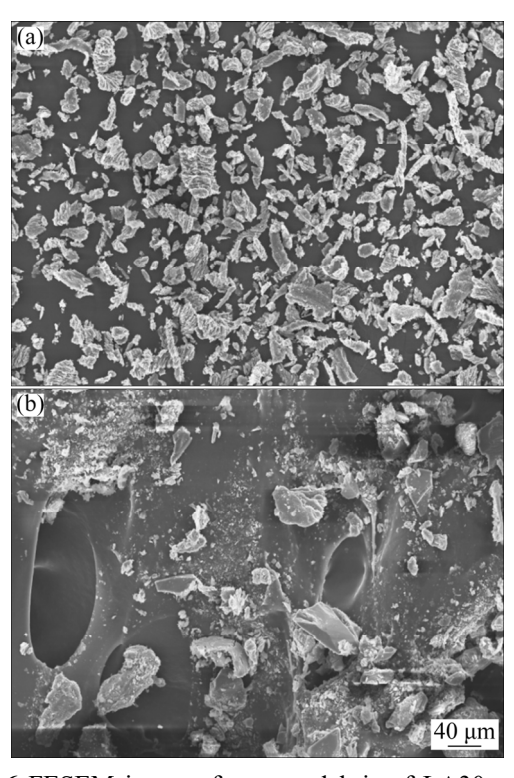


Fig. 6 FESEM images for wear debris of LA30 matrix alloy (a) and LA30–10%SiC composite (b) at abrasive size of 80 μ m and applied load of 7 N

5 Conclusions

- (1) The microstructure of LM30 alloy shows primary aluminium dendritic morphology, primary silicon cuboids, and eutectic silicons observed as needle-shape, grow isotropically as a result of a twin-plane re-entrant edge (TPRE) mechanism.
- (2) The microstructure of the composite exhibits a uniform dispersion of SiC particles and excellent interfacial bonding between the SiC particles and the matrix.
- (3) The hardness of the composite is 17% greater than that of the matrix alloy, as a result of adding SiC particles to the matrix.
- (4) The ultimate tensile strength (UTS) and yield strength (YS) of the composite are found to be

38% and 30% greater than those of the matrix alloy, respectively, and the elongation of the composite is 48% less than that of the matrix alloy. This may be due to the occurrence of a uniform dispersion of SiC particles and excellent interfacial bonding between the SiC particles and the matrix.

- (5) The wear rate increases with applied load and abrasive size and does not vary with the sliding distance.
- (6) The cutting, ploughing and delamination wear are the dominant wear mechanism in low load regime, and in high load regime, fragmentation, microcracking, micro fatigue and fracturing tendency are the dominant wear mechanism.

Acknowledgments

The authors would like to acknowledge the financial support received to the first author as a scholarship from MHRD, Government of India.

References

- [1] GARCÍA-INFANTA J M, ZHILYAEV A P, CEPEDA-JIMÉNEZ C M, RUANO O A, CARREÑO F. Effect of the deformation path on the ductility of a hypoeutectic Al–Si casting alloy subjected to equal-channel angular pressing by routes A, B_A, B_C and C [J]. Scripta Materialia, 2008, 58: 138–141.
- [2] KUCUKOMEROGLU T. Effect of equal-channel angular extrusion on mechanical and wear properties of eutectic Al–12Si alloy [J]. Materials & Design, 2010, 31: 782–789.
- [3] ELMADAGLI M, PERRY T, ALPAS A T. A parametric study of the relationship between microstructure and wear resistance of Al–Si alloys [J]. Wear, 2007, 262: 79–92.
- [4] SAHEB N, LAOUI T, DAUD A R, HARUN M, RADIMAN S, YAHAYA R. Influence of Ti addition on wear properties of Al–Si eutectic alloys [J]. Wear, 2001, 249: 656–662.
- [5] CEPEDA-JIMÉNEZ C M, GARCÍA-INFANTA J M, ZHILYAEV A P, RUANO O A, CARREÑO F. Influence of the thermal treatment on the deformation-induced precipitation of a hypoeutectic Al-7wt.%Si casting alloy deformed by high-pressure torsion [J]. Journal of Alloys and Compounds, 2011, 509: 636-643.
- [6] HERNÁNDEZ F C R, SOKOLOWSKI J H. Effects and on-line prediction of electromagnetic stirring on microstructure refinement of the 319 Al-Si hypoeutectic alloy [J]. Journal of Alloys and Compounds, 2009, 480: 416–421.
- [7] CAVALIERE P, CERRI E, LEO P. Effect of heat treatments on mechanical properties and damage evolution of thixoformed aluminium alloys [J]. Materials Characterization, 2005, 55: 35–42.
- [8] MA A, SUZUKI K, NISHIDA Y, SAITO N, SHIGEMATSU I, TAKAGI M, IWATA H, WATAZU A, IMURA T. Impact toughness of an ultrafine-grained Al-11mass%Si alloy

- processed by rotary-die equal-channel angular pressing [J]. Acta Materialia, 2005, 53: 211–220.
- [9] OZDEMIR I, MUECKLICH S, PODLESAK H, WIELAGE B. Thixoforming of AA2017 aluminum alloy composites [J]. Journal of Materials Processing Technology, 2011, 211: 1260–1267.
- [10] SAWLA S, DAS S. Combined effect of reinforcement and heat treatment on the two-body abrasive wear of aluminum alloy and aluminum particle composite [J]. Wear, 2004, 257: 555–561.
- [11] DAS S, MONDAL D P, DIXIT G. Correlation of abrasive wear with microstructure and mechanical properties of pressure die-cast aluminum hard-particle composite [J]. Metallurgical and Materials Transactions A, 2001, 32: 633–642.
- [12] RAAFT M, MAHMOUD T S, ZAKARIA H M, KHALIFA T A. Microstructural, mechanical and wear behavior of A390/graphite and A390/Al₂O₃ surface composites fabricated using FSP [J]. Materials Science and Engineering A, 2011, 528: 5741-5746.
- [13] MONDAL D P, DAS S. High stress abrasive wear behaviour of aluminium hard particle composites: Effect of experimental parameters, particle size and volume fraction [J]. Tribology International, 2006, 39: 470–478.
- [14] SHAH K B, KUMAR S, DWIVEDI D K. Aging temperature and abrasive wear behaviour of cast Al–(4%,12%,20%)Si–0.3%Mg alloys [J]. Materials & Design, 2007, 28: 1968–1974.
- [15] SINGH M, MONDAL D P, MODI O P, JHA A K. Two-body abrasive wear behaviour of aluminium alloy–sillimanite particle reinforced composite [J]. Wear, 2002, 253: 357–368.
- [16] GODE C, YILMAZER H, OZDEMIR I, TODAKA Y. Microstructural refinement and wear property of Al-Si-Cu composite subjected to extrusion and high-pressure torsion [J]. Materials Science and Engineering A, 2014, 618: 377-384.
- [17] LIN Chong, WU Shu-sen, LÜ Shu-lin, ZENG Jin-biao, AN Ping. Dry sliding wear behavior of rheocast hypereutectic Al–Si alloys with different Fe contents [J]. Transactions of Nonferrous Metals Society of China, 2016, 26: 665–675.
- [18] LI Run-xia, LIU Lan-ji, ZHANG Li-jun, SUN Ji-hong, SHI Yuan-ji, YU Bao-yi. Effect of squeeze casting on microstructure and mechanical properties of hypereutectic Al–xSi alloys [J]. Journal of Materials Science and Technology, 2017, 33: 404–410.
- [19] MONDAL D P, DAS S, JHA A K, YEGNESWARAN A H. Abrasive wear of Al alloy–Al₂O₃ particle composite: A study on the combined effect of load and size of abrasive [J]. Wear, 1998, 223: 131–138.
- [20] DAS S, MONDAL D P, SAWLA S, DIXIT S. High stress abrasive wear mechanism of LM13-SiC composite under varying experimental conditions [J]. Metallurgical and Materials Transactions A, 2002, 33: 3031-3044.
- [21] PRASAD B K, DAS S, JHA A K, MODI O P, DASGUPTA R, YEGNESWARAN A H. Factors controlling the abrasive wear response of a zinc-based alloy silicon carbide particle composite [J]. Composites: Part A, 1997, 28: 301–308.
- [22] MOORE M A, DOUTHWAITE R M. Plastic deformation

- below worn surfaces [J]. Metallurgical and Materials Transactions A, 1976, 7: 1833–1839.
- [23] PRASAD B K. Abrasive wear characteristics of a zinc-based alloy and zinc-alloy/SiC composite [J]. Wear, 2002, 252: 250–263.
- [24] SINGH R K, TELANG A, DAS S. Microstructure, mechanical, and high-stress abrasive wear behaviour of as-cast and heat-treated Al-Si-SiC_p composite [J]. International Journal of Materials Research, 2019, 110: 121–129.
- [25] PRASAD B K, JHA A K, MODI O P, DAS S, YEGNESWARAN A H. Abrasive wear characteristics of Zn-37.2Al-2.5Cu-0.2Mg alloy dispersed with silicon carbide particles [J]. Materials Transactions JIM, 1995, 36: 1048-1057.
- [1] PRASAD B K, VENKATESWARLU K, DAS S, JHA A K, DASGUPTA R. Influence of SiC reinforcement on the abrasive wear response of an Al-Cu alloy under conditions of varying abrasive size and applied load [J]. Journal of Materials Science Letters, 1997, 16: 1113–1115.

Al-Si-SiC 过共晶复合材料的显微组织、 力学性能和二体磨料磨损行为

Raj Kumar SINGH¹, Amit TELANG¹, Satyabrata DAS²

- Department of Mechanical Engineering, Maulana Azad National Institute of Technology, Link Road Number 3, Bhopal 462003, India;
- 2. Advanced Materials and Processes Research Institute (AMPRI), Near Habibganj Naka, Bhopal 462026, India

摘 要:采用搅拌铸造法制备过共晶 Al-Si-SiC 复合材料,研究该复合材料及其基体合金的显微组织、力学性能以及滑动距离和材料去除机理对材料二体磨料磨损行为的影响。结果表明,与基体合金相比,复合材料的硬度、极限抗拉强度和屈服强度分别提高 17%、38%和 30%,而伸长率降低 48%。材料的磨损率随磨料粒度和载荷的增大而增大,不随滑动距离的变化而变化。通过高分辨场发射扫描电镜(HR FESEM)对材料的磨损表面和磨屑进行表征,分析材料在高、低载荷状态下的磨损机理。

关键词: 金属基复合材料; 断面; 磨屑分析; 二体磨料磨损

(Edited by Wei-ping CHEN)